Mon. Not. R. Astron. Soc. **000**, 1–7 (2014) Printed 6 March 2015 (MN LATEX style file v2.2)

The hyperluminous X-ray source candidate in IC 4320: another HLX bites the dust

Andrew D. Sutton,[1,2⋆] Timothy P. Roberts,[1] Jeanette C. Gladstone,[3] Dominic J. Walton[4]

[1] *Department of Physics, University of Durham, South Road, Durham, DH1 3LE, UK*
[2] *Astrophysics Office, NASA Marshall Space Flight Center, ZP12, Huntsville, Al 35812, USA*
[3] *Department of Physics, University of Alberta, 11322-89 Avenue, Edmonton, Alberta T6G 2G7, Canada*
[4] *Space Radiation Laboratory, California Institute of Technology, Pasadena, CA 91125, USA*

6 March 2015

ABSTRACT

The known members of the class of hyperluminous X-ray sources (HLXs) are few in number, yet they are of great interest as they are regarded as the likeliest intermediate-mass black hole (IMBH) candidates amongst the wider population of ultraluminous X-ray sources (ULXs). Here we report optical photometry and spectroscopy of a HLX candidate associated with the galaxy IC 4320, that reveal it is a background AGN. We discuss the implications of the exclusion of this object from the small number of well-studied HLXs, that appears to accentuate the difference in characteristics between the good IMBH candidate ESO 243-49 HLX-1 and the small handful of other HLXs.

Key words: accretion, accretion discs – black hole physics – X rays: binaries – X rays: galaxies

1 INTRODUCTION

Hyperluminous X-ray sources (HLXs) are a subset of the brightest ultraluminous X-ray sources (ULXs). They are defined as point sources with X-ray luminosities in excess of 10^{41} erg s^{-1}, located away from the nucleus of external galaxies (Gao et al. 2003). However, they remain poorly understood compared to their lower-luminosity relations, for which substantial progress has been made in recent years. In particular, it has now been demonstated that at least three individual ULXs are powered by super-Eddington accretion onto stellar-mass black holes, with these objects located in the galaxies M31, M101 and NGC 7793 (Middleton et al. 2013; Liu et al. 2013; Motch et al. 2014). The last of these detections is crucial in understanding the wider population of ULXs as this object shows that the key spectral and behavioural differences between ULXs and sub-Eddington stellar-mass black holes (e.g. Gladstone, Roberts & Done 2009; Sutton, Roberts & Middleton 2013; see also Feng & Soria 2011 and references therein, with recent confirmation of the spectral differences coming from *NuSTAR* observations, e.g. Bachetti et al. 2013; Walton et al. 2013) manifest at super-Eddington rates. However, it is not yet clear whether HLXs can be produced in this way. It is therefore intriguing that luminosities up to $\sim 2 \times 10^{41}$ erg s^{-1} may be possible, from a combination of the most massive stellar remnant black holes (up to $\sim 80\ M_{\odot}$ in regions of low metallicity; Zampieri & Roberts 2009; Belczynski et al. 2010; Mapelli et al. 2010), and maximal super-Eddington accretion rates ($\sim 20\ L_{\rm Edd}$ from a face-on disc; Ohsuga & Mineshige 2011).

Alternatively, HLXs may harbour a new class of black hole – the intermediate-mass black holes (IMBHs; Colbert & Mushotzky 1999; 10^2–$10^4\ M_{\odot}$). To produce the observed X-ray luminosities while accreting in standard sub-Eddington states requires HLXs to host IMBHs with masses of $> 10^3\ M_{\odot}$. Indeed, there is arguably good evidence that this is the case in the most luminous HLX, ESO 243-49 HLX-1 ($L_{\rm X,peak} \sim 10^{42}$ erg s^{-1}, Farrell et al. 2009; although see King & Lasota 2014 and Lasota, King & Dubus 2015 for an alternative scenario). This source exhibits regular outbursts, which appear to have a fast rise, exponential decay (FRED) profile, repeated on a timescale of ~ 1 year (Lasota et al. 2011; but see Godet et al. 2013). Most crucially, its behaviour on the hardness-intensity diagram as it progresses through these outbursts appears to mimic sub-Eddington black hole binaries (Servillat et al. 2011). It has been suggested that the putative IMBH in ESO 243-49 HLX-1 may have originated in the nucleus of a stripped satellite dwarf galaxy, whose host has been disrupted in an encounter

⋆ Email: andrew.d.sutton@nasa.gov

with the larger galaxy, or a large black hole recoiling from a close encounter with the nuclear black hole of ESO 243-49 (Soria, Hau & Pakull 2013).

There are very few other sources that join ESO 243-49 HLX-1 in the category of confirmed or even potential HLXs. The best candidates include M82 X-1 (Matsumoto et al. 2001), Cartwheel N10 (Gao et al. 2003; Wolter & Trinchieri 2004), 2XMM J011942.7+032421 in NGC 470 and 2XMM J134404.1−271410 in IC 4320 (Walton et al. 2011; Sutton et al. 2012), the last of which we consider further in this paper. Several other candidate HLXs have been mooted, but the evidence for these is less conclusive. They include n40 in NGC 5775, which was estimated by Ghosh et al. (2009) to have an intrinsic X-ray luminosity of $L_{\rm X} \sim 10^{41}$ erg s^{-1}, although its observed luminosity was nearer 7.5×10^{40} erg s^{-1}. Also included is CXO J122518.6+144545, which has an intrinsic 0.5–10 keV luminosity of $L_{\rm X} \sim 2.7 \times 10^{41}$ erg s^{-1}, if it is at the distance of its presumed host galaxy. However, in this case a blue Type IIn supernova or a recoiling SMBH offer viable alternative solutions (Jonker et al. 2010). Davis & Mushotzky (2004) identified 2XMM J072647.9+854550 in NGC 2276 as a potential HLX, at $L_{\rm X} \sim 1.1 \times 10^{41}$ erg s^{-1}. But, this object has been both resolved into a triplet of ULXs by *Chandra* observations, and its luminosity revised down based on a more recent distance measurement, such that it is no longer hyperluminous (Wolter et al. 2011; Sutton et al. 2012), although a recent X-ray/radio fundamental plane measurement highlights this ULX as a very strong IMBH candidate (Mezcua et al. 2015). Several other HLX candidates have been categorically ruled out. XMMU J132218.3−164247 (Miniutti et al. 2006) turned out to be a type 1 QSO at $z \sim 1$ (Dadina et al. 2013), and Sutton et al. (2012) identified two further HLX candidates from the 2XMM catalogue – 2XMM J120405.8+201345 and 2XMM J125939.8+275718 – as background QSOs.

Given the scarcity of these objects, it is important that we properly scrutinise each potential source. Here we focus on 2XMM J134404.1−271410, the HLX candidate in IC 4320. At an X-ray luminosity of $L_{\rm X} = 3.5^{+0.2}_{-0.3} \times 10^{41}$ erg s^{-1} (if it is at the distance of IC 4320), it is potentially second only in peak luminosity amongst all HLXs to ESO 243-49 HLX-1. Even at this extreme luminosity, it has been observed in an apparent low/hard X-ray state, making it an excellent IMBH candidate (Sutton et al. 2012). As such, it is critical to confirm whether this source is indeed associated with IC 4320.

In this work, we report on VLT imaging and spectroscopic observations of 2XMM J134404.1−271410. We present the data in section 2, and show that they rule this source out as a potential HLX. In section 3 we discuss the physical interpretation of the dwindling HLX population.

2 ANALYSIS AND RESULTS

The region around IC 4320 was observed with VLT VIMOS in imaging mode, using the *UBVRI* filters. Details of these observations are given in Table 1, and they are available

Table 1. VLT VIMOS exposures

Obs. ID[a]	Filter[b]	Date[c]	$N^d_{\rm exp}$	$t^e_{\rm exp}$
822880	*U*	2013-02-12 09:09:00	3	69
	I	2013-02-12 09:17:21	3	301
786873	*B*	2013-02-14 08:09:36	3	245
	V	2013-02-14 08:26:35	3	344
786878	*R*	2013-02-15 08:20:12	3	501

Details of the VIMOS photometric exposures of 2XMM J134404.1−271410, taken using VLT UT3, as part of VLT observing run 090.D-0300(A). [a]Observation identifier. [b]VLT VIMOS broad band filter in which the observation was taken. [c]Start date and time of the first exposure in the series (YYYY-MM-DD HH:MM:SS). [d]Total number of consecutive exposures with the same filter. [e]Exposure time of each of the $N_{\rm exp}$ exposures (s).

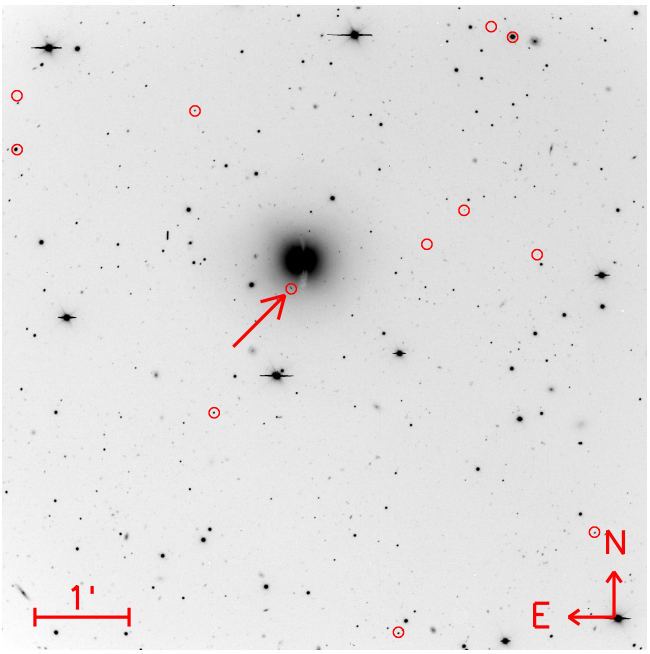

Figure 1. Logarithmically scaled *V*-band VIMOS image of the region around IC 4320. The positions of nearby X-ray sources are shown with arbitrarily-sized red circles. These were identified from the *Chandra* data, and used to correct the relative astrometry of the images. The red arrow indicates the *Chandra* position of 2XMM J134404.1−271410.

Table 2. VLT FORS2 exposures

Obs. ID[a]	Date[b]	$N^c_{\rm exp}$	$t^d_{\rm exp}$
1000792	2014-03-10 06:15:15	2	1360
1000795	2014-03-12 05:29:45	2	1360

Details of the FORS2 long slit spectral exposures of 2XMM J134404.1−271410, taken using VLT UT1, as part of VLT observing run 092.D-0212(A). All of the exposures were taken using the 0.7 arcsecond slit, the GRIS300V+10 grism and the GG435 filter. [a]Observation identifier. [b]Start date and time of the first exposure in the series (YYYY-MM-DD HH:MM:SS). [c]Total number of consecutive exposures. [d]Exposure time of each of the $N_{\rm exp}$ exposures (s).

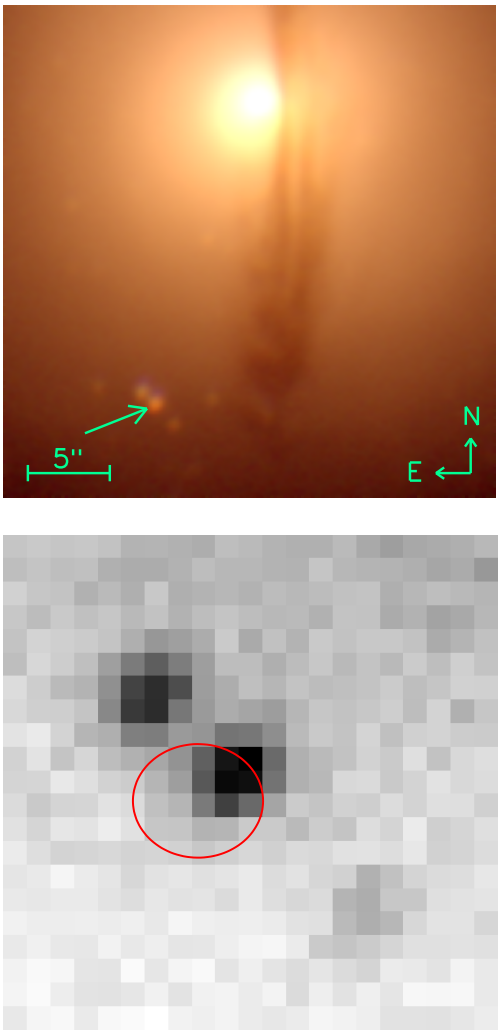

Figure 2. (*top*) Smoothed, true colour image showing the region around 2XMM J134404.1−271410. The RGB colours correspond to the *RVB* VLT VIMOS bands, and the green arrow shows the counterpart, which was the target of a subsequent series of VLT FORS2 long slit spectral observations. (*bottom*) Close-up, unsmoothed VLT VIMOS V-band image of the region close to the ULX. The red ellipse indicates the 3σ *Chandra* uncertainty region of the X-ray point source, after correcting for the relative astrometry of the X-ray and optical images.

in the ESO data archive.[1] The science exposures and associated calibration files were reduced using the standard tools in the VLT VIMOS pipeline (version 2.9.1), along with the common pipeline library (CPL; version 6.1.1),[2] in GASGANO (version 2.4.3).[3] In order to identify any counterpart to the HLX candidate, we needed to align the VIMOS image with an X-ray image. To do this, we used data from a 50 ks *Chandra* ACIS-S observation (observation ID 12989), previously reported in Sutton et al. (2012). We detected X-ray sources in a 0.5-7 keV image using WAVDETECT in CIAO (version 4.4)[4], focussing on a 6 arcminute region around 2XMM J134404.1−271410. Excluding the HLX candidate, 11 X-ray sources were detected in the same VIMOS quadrant as the target. These sources were used to align the relative astrometry of the X-ray and optical images (Figure 1), via the IRAF tools CCFIND, CCMAP and CCWCS. In this way, we were able to constrain the relative right ascension and declination corrections to ± 0.181 and 0.158 arcsecond respectively. These values were combined with the ∼ 0.01 arcsecond error in the centroid position of the *Chandra* source to calculate a combined (3σ) uncertainty region with semi-major and minor axes of ∼ 0.5 arcsecond. Having done this, we were able to identify an optical source that was coincident with 2XMM J134404.1−271410 (Figure 2). This counterpart had (Galactic-reddening-corrected) apparent Vega magnitudes of $m_U = 24.5\pm0.6$, $m_B = 23.16\pm0.07$, $m_V = 22.67\pm0.05$, $m_R = 21.51\pm0.05$ and $m_I = 20.8\pm0.2$. If the source is indeed associated with IC 4320, then it would have a distance modulus of ∼ 34.89, and the counterpart would be both brighter and redder than that of ESO 243-49 HLX-1 (Soria et al. 2012; Farrell et al. 2012).

Having identified an optical counterpart, it was critical to confirm whether it was indeed associated with IC 4320. To this end, we were awarded VLT FORS2 observing time to obtain a long slit spectrum, and hence measure the redshift of the source. Details of the FORS2 exposures are given in Table 2; these will be available in the ESO archive following the 1 year proprietary period. The observations and associated calibration files were processed using FORS_BIAS, FORS_CALIB and FORS_SCIENCE, as part of the FORS pipeline (version 4.11.13), with the CPL (version 6.3). Initially, FORS_SCIENCE was used to process standard star observations of Feige 66 to produce spectral response curves for the instrument configuration. These spectral response curves were then used as inputs to the FORS_SCIENCE pipeline when processing the science exposures, to allow us to produce flux-calibrated spectra for each exposure. Finally, we median combined the individual flux-calibrated science spectra.

The VLT FORS2 spectrum is shown in Figure 3. There are clearly a number of broad emission lines, which suggest that the source contains a type-1 active galactic nucleus (AGN). We fitted these emission lines with Gaussian profiles using SPLAT,[5] and measured their wavelengths and line widths. The centroids of the emission lines are constrained to be at 4669±1, 4758±3, 5949±1 and 7329±4 Å, with FWHMs of 54 ± 3, 60 ± 10, 64 ± 3 and 90 ± 10 Å respectively. These lines are consistent with the Lyman α 1216 Å, N V 1240 Å, C IV 1549 Å and C III 1909 Å lines respectively, if at a redshift of ∼ 2.84, with velocity dispersions of ∼ 3000 km s^{-1}. We can therefore confidently exclude 2XMM J134404.1−271410 from being a HLX associated with the galaxy IC 4320; instead we identify it as a background QSO. We calculate a luminosity distance of $\sim 2.4 \times 10^4$ Mpc to the QSO, for $H_0 = 71$, $\Omega_{\rm M} = 0.27$ and $\Omega_{\rm vac} = 0.73$. At this distance, 2XMM J134404.1−271410 has a peak observed 0.3–10 keV (rest frame 1.15–38.4 keV) luminosity of $\sim 2.2\times10^{46}$ erg s^{-1} (calculated using the peak 0.3–10 keV observed flux from

[1] archive.eso.org
[2] www.eso.org/sci/software/pipelines/
[3] www.eso.org/sci/software/gasgano.html
[4] cxc.harvard.edu/ciao
[5] http://star-www.dur.ac.uk/~pdraper/splat/splat-vo/splat-vo.html

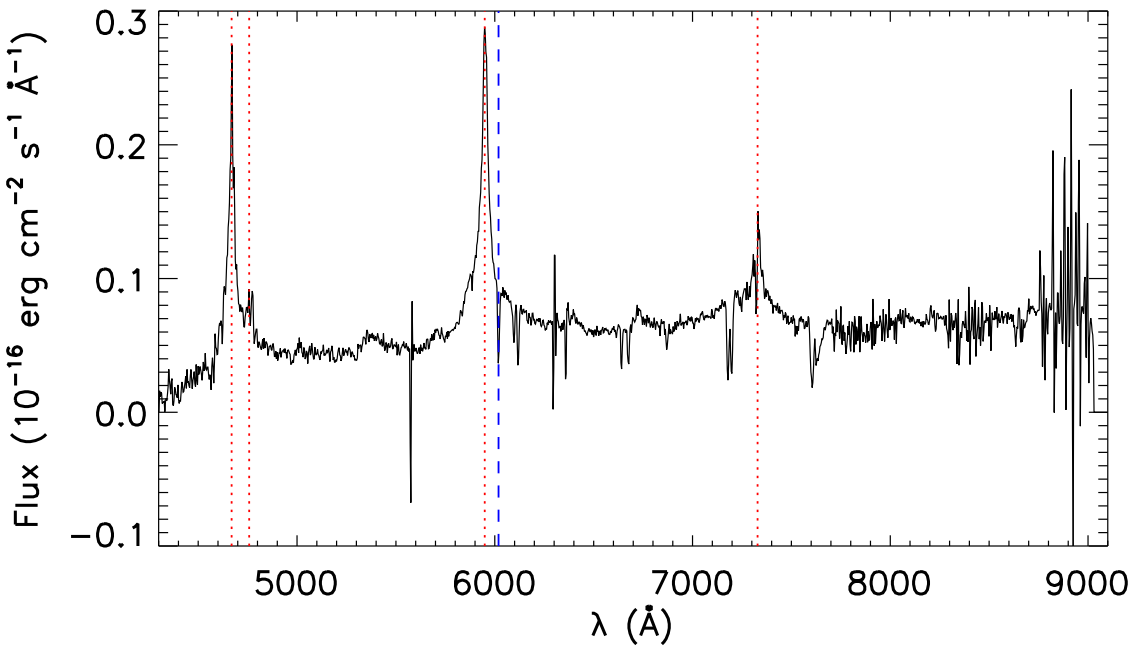

Figure 3. VLT FORS2 long slit spectrum of the optical counterpart to 2XMM J134404.1−271410. We identify the broad emission lines (dotted red lines) as (from low to high wavelength) Lyman α, N v, C iv and C iii. From these we calculate a redshift of ~ 2.84. Several absorption features can also be observed. The (unmarked) narrow features at ~ 5579 and 6302 Å, and the broad feature around 7600 Å are telluric. We tentatively identify the 6019 Å absorption line (blue dashed line) as being consistent with neutral sodium in IC 4320, whilst the other unidentified absorption features may originate in one or more absorbers along the line-of-sight to the optical emission.

Sutton et al. 2012); this is not unusually luminous for a redshift ~ 3 source (cf. Ueda et al. 2014).

It is possible to obtain an estimate of the black hole mass from the FWHM of the C iv line and the continuum luminosity. Here, we do this for 2XMM J134404.1−271410 using the relation from Vestergaard & Peterson (2006):

$$\log M_{\rm BH}({\rm C\ IV}) = \log\left\{\left[\frac{\rm FWHM(C\ IV)}{1000\ {\rm km\ s^{-1}}}\right]^2 \times \left[\frac{\lambda L_\lambda(1450{\rm \AA})}{10^{44}\ {\rm erg\ s^{-1}}}\right]^{0.53}\right\} + (6.73 \pm 0.01). \quad (1)$$

This process is slightly complicated by the fact that the 1450 Å luminosity at the redshift of the emission lines is close to the 5579 Å skyline. As such, we estimate the continuum luminosity at a rest frame wavelength of 1450 Å by extrapolating the spectrum from either side of the 5579 Å absorption feature. We estimate a black hole mass of $\sim 2\times10^8 M_\odot$, which is indicative of an Eddington ratio of ~ 1. However, we note that the C iv black hole mass estimate is subject to a high degree of systematic uncertainty. Not only is there no common procedure for fitting the emission line, as it is confused with other sources of emission (e.g. Fine et al. 2010), but it may also be subject to non-gravitational effects (Baskin & Laor 2005).

In addition to the emission lines, there are also a number of absorption features in the FORS2 spectrum. As above, we measured their wavelengths using SPLAT, and checked whether these features were consistent with originating at the emission line redshift, or that of IC 4320. After eliminating a number of telluric features, we tentatively identifed an absorption feature at 6019.2 ± 0.4 Å as originating from neutral Na in IC 4320 (Figure 3). We suggest that the other unidentified features may originate in one or more intervening absorbers.

3 DISCUSSION

Although now recognised as highly interesting objects, given that they appear good candidates for hosting IMBHs, the number of *bona fide* HLXs remains small. With our identification of one of the best remaining HLX candidates, 2XMM J134404.1–271410, as a background QSO, their scarcity is emphasised further. In this section we therefore consider what the properties of the few remaining objects in this class might tell us about their nature.

But first, it is interesting with hindsight to speculate whether 2XMM J134404.1−271410 could have been rejected as a potential ULX based on its X-ray to optical flux ratio. We use the optical magnitude in the V-band, along with the *Chandra* flux (calculated from a power-law model; see Sutton et al. 2012 for details) to estimate the X-ray to optical flux ratio of the target. We use the Stocke et al. (1991) definition of the flux ratio ($\log(f_{\rm X}/f_{\rm opt}) \equiv \log f_{0.3-3.5{\rm keV}} + m_V/2.5 + 5.37$), to obtain $\log(f_{\rm X}/f_{\rm opt}) = 1.67 \pm 0.2$. This sits between the ranges of X-ray to optical flux ratios for typical AGN (-1 – 1.2; Stocke et al. 1991) and ULXs (2 – 3;

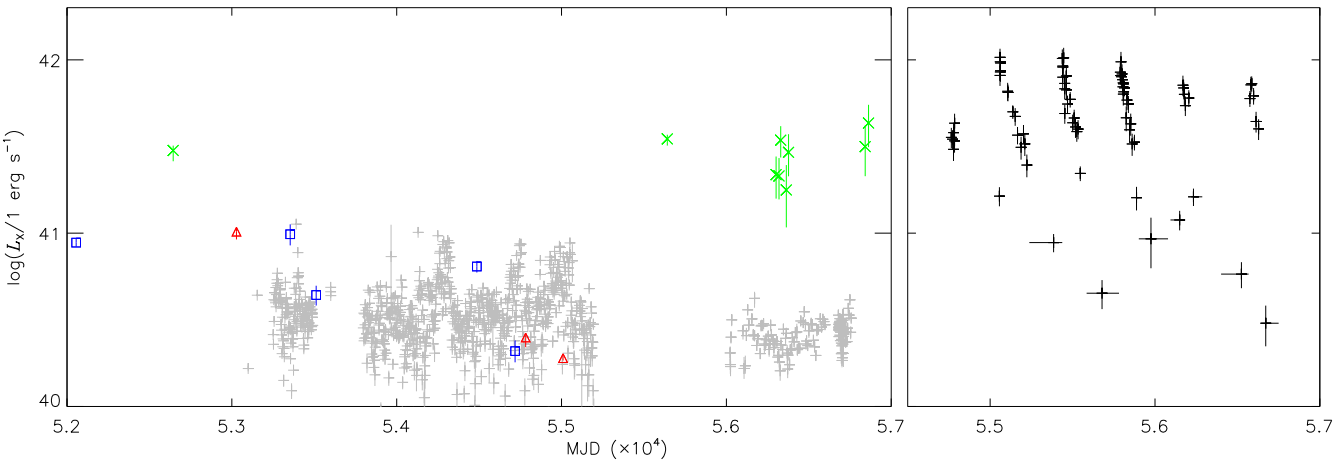

Figure 4. (*left*) Long term light curve showing 2XMM J134404.1−271410 (green diagonal crosses) under the incorrect assumption that it is at the distance of IC 4320, and three of the remaining good HLX candidates. The sources are Cartwheel N10 (blue squares), 2XMM J011942.7+032421 in NGC 470 (red triangles) and M82 X-1 (grey crosses). The data for 2XMM J134404.1−271410 are 0.3–10 keV observed luminosities. They include the *XMM-Newton* and *Chandra* detections reported in Sutton et al. (2012), plus several *Swift* XRT observations. 0.3–10 keV count rates were extracted from the *Swift* data, then converted to luminosities using PIMMS and an assumed absorbed power-law spectrum, with parameters from Sutton et al. (2012). The data for 2XMM J011942.7+032421 are 0.3–10 keV observed luminosities taken from Sutton et al. (2012). The Cartwheel N10 data were estimated from Figure 4 of Pizzolato, Wolter & Trinchieri (2010), and converted to 0.3–10 keV observed luminosities using a distance of 122 Mpc (Wolter & Trinchieri 2004) and the power-law spectral fits reported in Pizzolato, Wolter & Trinchieri (2010). The M82 X-1 data are from *RXTE* PCA and *Swift* XRT observations taken in photon counting mode. For the *RXTE* observations, we used count rates from the archival mission-long light curve. We then estimated a conversion factor to 0.3–10 keV observed luminosities using PIMMS, for an absorbed power law model with $N_{\rm H} = 1.12 \times 10^{22}$ cm^{-2} and $\Gamma = 1.67$ (Kaaret, Simet & Lang 2006). For the *Swift* data, we extracted 2–10 keV background subtracted spectra using XSELECT, and fitted these with an absorbed power-law model in XSPEC. The absorption column density and power-law spectral index were fixed to the values from Kaaret, Simet & Lang (2006). The choice of the 2–10 keV bandpass was due to the necessity of reducing contamination from diffuse emission in the M82. We extrapolated the absorbed power-law to the full 0.3–10 keV band, to estimate the observed flux. M82 X-1 is not resolved from other nearby point sources by *Swift* or *RXTE*, so the values that we obtain are effectively upper-limits on the flux from X-1. The second brightest point source in the extraction region is M82 X-2, which at its peak is around half as luminous as X-1 (Miyawaki et al. 2009). (*right*) Light curve showing the FRED profile of ESO 243-49 HLX-1, shown on the same time scale. 0.3–10 keV count rates were extracted from *Swift* XRT data, and were grouped in to bins of 50 counts. These count rates were converted to estimated luminosities by assuming a bimodal distribution of X-ray spectra, with typical parameters taken from Servillat et al. (2011). Below 5×10^{-3} cts s^{-1} an absorbed power-law spectrum was assumed, with $N_{\rm H} = 3 \times 10^{20}$ cm^{-2} and $\Gamma = 2.1$. At higher count rates, ESO 243-49 HLX-1 was assumed to have an absorbed multi-colour-disc spectrum, with $N_{\rm H} = 3 \times 10^{20}$ cm^{-2} and $kT = 0.22$ keV.

Tao et al. 2011). Such a high flux ratio could be indicative of an obscured QSO at high redshift, as X-ray absorption decreases strongly at high energies, whilst dust extinction increases toward the UV. Indeed, Fiore et al. (2003) report that the X-ray to optical flux ratio roughly scales as $(1+z)^{3.6}$ (albeit in different X-ray and optical bands). If this relation approximately holds for the definition of the X-ray to optical flux ratio that we use here, then we would expect $\log(f_{\rm X}/f_{\rm opt}) \sim 0$ at $z \sim 0$, which is entirely consistent with a QSO. However, we note that a few ULXs do have values of $\log(L_{\rm X}/L_{\rm opt}) < 2$ (Tao et al. 2011; Heida et al. 2013), thus neither identification could be categorically ruled out based on X-ray to optical flux ratio alone.

Before its exclusion as a HLX, 2XMM J134404.1−271410 provided an interesting bridge between ESO 243-49 HLX-1 and the other HLX candidates. Aside from being intermediate in peak luminosity between ESO 243-49 HLX-1 and other HLXs, it was also the only other HLX candidate to (apparently) reside in an early-type galaxy. In fact, both its apparent host (IC 4320) and that of ESO 243-49 HLX-1 are lenticular galaxies that host a dust lane (e.g. Farrell et al. 2012; cf. Fig. 2). In contrast, the other good, relatively nearby HLX candidates are located in late-type hosts (de Vaucouleurs et al. 1991): a ring galaxy (Cartwheel N10); an interacting SA(rs)b (NGC 470, 2XMM J011942.7+032421; with the association between the galaxy and HLX being confirmed by Gutiérrez & Moon 2014); and an edge-on I0 galaxy (M82 X-1). In fact, the location of these three less luminous HLXs is strongly reminiscent of the ordinary ULX population, as is the case for most of the extreme ULXs ($L_{\rm X} > 5 \times 10^{40}$ erg s^{-1}; Sutton et al. 2012), and indeed both the Cartwheel and M82 also host several fainter ULXs (e.g. Gao et al. 2003; Wolter & Trinchieri 2004; Kaaret, Simet & Lang 2006). So, by excluding the IC 4320 object, ESO 243-49 HLX-1 appears more strongly distinguished from the other HLXs in terms of its host system.

One characteristic that should perhaps have marked 2XMM J134404.1−271410 out as different to other HLXs was its relatively persistent X-ray luminosity, not varying much from $\sim 3 \times 10^{41}$ erg s^{-1} (under the misapprehension it is associated with IC 4320; Sutton et al. 2012; cf. Fig. 4). This behaviour is not seen in the other reasonably well-studied HLXs, that we show are all far more variable

over comparable time scales in Fig. 4. Of these, ESO 243-49 HLX-1 is unique in displaying a well constrained FRED-like outburst cycle (Lasota et al. 2011). It is also the only remaining source that is observed to exceed $\sim 2\times10^{41}$ erg s^{-1} (Farrell et al. 2009). M82 X-1 has been extensively monitored with both *RXTE* and *Swift*; it exhibits multiple epochs of flaring (e.g. Pasham & Strohmayer 2013), which can peak at $\sim 10^{41}$ erg s^{-1}, and was reported to have a possible 62 day period in *RXTE* observations (Kaaret & Feng 2007), although it is now thought that this is probably superorbital in nature (Pasham & Strohmayer 2013). The X-ray lightcurves of Cartwheel N10 and 2XMM J011942.7+032421 are not as well sampled. However, similarly to M82 X-1, we do know that they are not persistently hyperluminous, rather they can appear with substantially diminished fluxes in subsequent epochs (Wolter, Trinchieri & Colpi 2006; Pizzolato, Wolter & Trinchieri 2010; Sutton et al. 2012).

It is also important to consider the X-ray spectra of the HLX candidates. 2XMM J134404.1−271410 was considered a good IMBH candidate, as it had a low/hard state-like spectrum whilst appearing to be a HLX (although in retrospect this was also consistent with an AGN-like spectrum). In contrast, 2XMM J011942.7+032421 has been reported to have a curved, disc-like X-ray spectrum when it is at its most luminous, but to appear more power-law-like when faded below its peak luminosities (Sutton et al. 2012). The X-ray spectrum of Cartwheel N10 is inconclusive; archival data are relatively low quality and statistically well-fitted by both power-law and disc models (Pizzolato, Wolter & Trinchieri 2010). However, M82 X-1 does also show a trend of disc-like hard curvature when it is most luminous (Chiang & Kong 2011; Sazonov, Lutovinov & Krivonos 2014), with several authors arguing this is indicative of a sub-Eddington low/hard – high/soft state transition (e.g. Feng & Kaaret 2010; Chiang & Kong 2011). It is notable, however, for both M82 X-1 and 2XMM J011942.7+032421 the disc-like states have temperatures ~ 1 keV, more indicative of a stellar-mass black hole than a large IMBH.[6]

It is interesting to speculate, in light of 2XMM J134404.1−271410 being excluded from the HLX population, what the characteristics of the remaining sources tells us about the physical nature of HLXs. In ESO 243-49 HLX-1 there is arguably strong evidence from both the luminosity of the object and its behaviour for the presence of a 10^4–10^5 $M_\odot$ IMBH (e.g. Davis et al. 2011; Webb et al. 2012; although see Lasota, King & Dubus 2015 for another view on this object). The case for IMBHs in the other HLX candidates is not always as strong, with in particular M82 X-1 having many various black hole mass estimates (see e.g. Miyawaki et al. 2009; Pasham, Strohmayer & Mushotzky 2014). The exclusion of 2XMM J134404.1−271410 from the class of HLXs serves primarily to highlight the gulf in peak luminosity and behavioral properties between ESO 243-49 HLX-1 and the fainter HLXs. We note that the latter objects share a similar peak luminosity ($L_{\rm X} \sim 10^{41}$ erg s^{-1}; Figure 4), albeit in two cases from very sparsely sampled lightcurves, which is very close to the peak luminosity predicted for massive stellar black holes that are maximally accreting (see Section 1). They also share their host environments - young, star-forming regions - with the bulk of the less luminous ULX population. Their spectral properties are also interesting in this sense - in super-Eddington models, the spectra are predicted to become more disc-like at the highest luminosities as the radiatively-driven wind envelops the objects and Compton downscattering in the outflow dominates (Kawashima et al. 2012); this may be what is observed in M82 X-1 and 2XMM J011942.7+032421. (Interestingly, this phenomenon may also already have been seen in some standard ULXs as they reach their peak luminosities, e.g. Vierdayanti et al. 2010; Pintore & Zampieri 2012; Walton et al. 2014). This dichotomy in observed characteristics therefore leads us to speculate that we could be seeing two separate populations amongst the small number of HLXs: ESO 243-49 HLX-1 stands alone as an outstanding IMBH candidate, while the other objects may represent the absolute luminosity peak of the 'normal' X-ray binary population, powered by maximal hyper-Eddington accretion onto the largest stellar remnant black holes.

[6] We note however that very high disc temperatures are seen in a few Galactic black hole binaries in the steep power-law state (e.g., $kT = 2.7 - 3.8$ keV in 4U 1630-47; Tomsick et al. 2005). This would scale with the black hole mass as $M^{-1/4}$, thus corresponds to a disc temperature of ~ 1 keV for a $\sim 10^3$ $M_\odot$ IMBH.

4 CONCLUSIONS

In conclusion, in this paper we have demonstrated that 2XMM J134404.1−271410 is a background QSO and not a HLX associated with IC 4320. This causes the already small number of known HLX candidates in the local Universe to decline further, but perhaps more importantly it serves to emphasise the gulf in properties between the prototypical IMBH candidate, ESO 243-49 HLX-1, and the handful of other objects in the HLX class. We have argued that this may be due to a real physical difference between HLX-1 and the other objects; but clearly this is highly speculative, being based on a small number of rather poorly observed objects. Future missions with both the survey capability to detect more candidate HLXs (e.g. *eRosita*) and the collecting area and instruments to study this class in far greater detail (e.g. *Athena*) are required to make real progress in confirming or refuting our suspicions.

ACKNOWLEDGEMENTS

ADS and TPR acknowledge funding from the Science and Technology Facilities Council as part of the consolidated grants ST/K000861/1 and ST/L00075X/1. This work is based on observations made with ESO telescopes at the La Silla Paranal Observatory under programme IDs 090.D-0300(A) and 092.D-0212(A). It is also based in part on observations made by the *Chandra* X-ray Observatory, and made use of data supplied by the UK *Swift* Science Data Centre at the University of Leicester.

REFERENCES

Bachetti M., et al., 2013, ApJ, 778, 163
Baskin A., Laor A., 2005, MNRAS, 356, 1029

Belczynski K., Bulik T., Fryer C. L., Ruiter A., Valsecchi F., Vink J. S., Hurley J. R., 2010, ApJ, 714, 1217
Chiang Y.-K., Kong A. K. H., 2011, MNRAS, 414, 1329
Colbert E. J. M., Mushotzky R. F., 1999, ApJ, 519, 89
Dadina M., Masetti N., Cappi M., Malaguti G., Miniutti G., Ponti G., Gandhi P., De Marco B., 2013, A&A, 559, A86
Davis D. S., Mushotzky R. F., 2004, ApJ, 604, 653
Davis S. W., Narayan R., Zhu Y., Barret D., Farrell S. A., Godet O., Servillat M., Webb N. A., 2011, ApJ, 734, 111
de Vaucouleurs G., de Vaucouleurs A., Corwin, Jr. H. G., Buta R. J., Paturel G., Fouqué P., 1991, Third Reference Catalogue of Bright Galaxies. Volume I: Explanations and references. Volume II: Data for galaxies between 0^h and 12^h. Volume III: Data for galaxies between 12^h and 24^h. Springer-Verlag
Farrell S., et al., 2012, ApJL, 747, L13
Farrell S. A., Webb N. A., Barret D., Godet O., Rodrigues J. M., 2009, Nature, 460, 73
Feng H., Kaaret P., 2010, ApJL, 712, L169
Feng H., Soria R., 2011, New Astron. Rev., 55, 166
Fine S., Croom S. M., Bland-Hawthorn J., Pimbblet K. A., Ross N. P., Schneider D. P., Shanks T., 2010, MNRAS, 409, 591
Fiore F. et al., 2003, A&A, 409, 79
Gao Y., Wang Q. D., Appleton P. N., Lucas R. A., 2003, ApJL, 596, L171
Ghosh K. K., Saripalli L., Gandhi P., Foellmi C., Gutiérrez C. M., López-Corredoira M., 2009, AJ, 137, 3263
Gladstone J. C., Roberts T. P., Done C., 2009, MNRAS, 397, 1836
Godet O., Webb N., Barret D., Farrell S., Gehrels N., Servillat M., Soria R., 2013, The Astronomer's Telegram, 5439, 1
Gutiérrez C. M., Moon D.-S., 2014, ApJL, 797, L7
Heida M., Jonker P. G., Torres M. A. P., Roberts T. P., Miniutti G., Fabian A. C., Ratti E. M., 2013, MNRAS, 433, 681
Jonker P. G., Torres M. A. P., Fabian A. C., Heida M., Miniutti G., Pooley D., 2010, MNRAS, 407, 645
Kaaret P., Feng H., 2007, ApJ, 669, 106
Kaaret P., Simet M. G., Lang C. C., 2006, ApJ, 646, 174
Kawashima T., Ohsuga K., Mineshige S., Yoshida T., Heinzeller D., Matsumoto R., 2012, ApJ, 752, 18
King A., Lasota J.-P., 2014, MNRAS, 444, L30
Lasota J.-P., Alexander T., Dubus G., Barret D., Farrell S. A., Gehrels N., Godet O., Webb N. A., 2011, ApJ, 735, 89
Lasota J.-P., King A. R., Dubus G., 2015, ApJL, 801, L4
Liu J.-F., Bregman J. N., Bai Y., Justham S., Crowther P., 2013, Nature, 503, 500
Mapelli M., Ripamonti E., Zampieri L., Colpi M., Bressan A., 2010, MNRAS, 408, 234
Matsumoto H., Tsuru T. G., Koyama K., Awaki H., Canizares C. R., Kawai N., Matsushita S., Kawabe R., 2001, ApJL, 547, L25
Mezcua M., Roberts T. P., Lobanov A. P., Sutton A. D., 2015, MNRAS, 448, 1893
Middleton M. J. et al., 2013, Nature, 493, 187
Miniutti G., Ponti G., Dadina M., Cappi M., Malaguti G., Fabian A. C., Gandhi P., 2006, MNRAS, 373, L1
Miyawaki R., Makishima K., Yamada S., Gandhi P., Mizuno T., Kubota A., Tsuru T. G., Matsumoto H., 2009, PASJ, 61, 263
Motch C., Pakull M. W., Soria R., Grisé F., Pietrzyński G., 2014, Nature, 514, 198
Ohsuga K., Mineshige S., 2011, ApJ, 736, 2
Pasham D. R., Strohmayer T. E., 2013, ApJL, 774, L16
Pasham D. R., Strohmayer T. E., Mushotzky R. F., 2014, Nature, 513, 74
Pintore F., Zampieri L., 2012, MNRAS, 420, 1107
Pizzolato F., Wolter A., Trinchieri G., 2010, MNRAS, 406, 1116
Sazonov S. Y., Lutovinov A. A., Krivonos R. A., 2014, Astronomy Letters, 40, 65
Servillat M., Farrell S. A., Lin D., Godet O., Barret D., Webb N. A., 2011, ApJ, 743, 6
Soria R., Hakala P. J., Hau G. K. T., Gladstone J. C., Kong A. K. H., 2012, MNRAS, 420, 3599
Soria R., Hau G. K. T., Pakull M. W., 2013, ApJL, 768, L22
Stocke J. T., Morris S. L., Gioia I. M., Maccacaro T., Schild R., Wolter A., Fleming T. A., Henry J. P., 1991, ApJS, 76, 813
Sutton A. D., Roberts T. P., Middleton M. J., 2013, MNRAS, 435, 1758
Sutton A. D., Roberts T. P., Walton D. J., Gladstone J. C., Scott A. E., 2012, MNRAS, 423, 1154
Tao L., Feng H., Grisé F., Kaaret P., 2011, ApJ, 737, 81
Tomsick J. A., Corbel S., Goldwurm A., Kaaret P., 2005, ApJ, 630, 413
Ueda Y., Akiyama M., Hasinger G., Miyaji T., Watson M. G., 2014, ApJ, 786, 104
Vestergaard M., Peterson B. M., 2006, ApJ, 641, 689
Vierdayanti K., Done C., Roberts T. P., Mineshige S., 2010, MNRAS, 403, 1206
Walton D. J. et al., 2013, ApJ, 779, 148
Walton D. J. et al., 2014, ApJ, 793, 21
Walton D. J., Roberts T. P., Mateos S., Heard V., 2011, MNRAS, 416, 1844
Webb N. et al., 2012, Science, 337, 554
Wolter A., Pizzolato F., Rota S., Mapelli M., Ripamonti E., 2011, AN, 332, 358
Wolter A., Trinchieri G., 2004, A&A, 426, 787
Wolter A., Trinchieri G., Colpi M., 2006, MNRAS, 373, 1627
Zampieri L., Roberts T. P., 2009, MNRAS, 400, 677

This paper has been typeset from a TEX/ LATEX file prepared by the author.